Q. J. R. Meteorol. Soc. **00**: 2–11 (2008)
Published online in Wiley InterScience
(www.interscience.wiley.com) DOI: 10.1002/qj.000

The diurnal cycle of surface divergence over the global oceans

R. Wood[a]*, M. Köhler[b], R. Bennartz[c] and C. O'Dell[c]
[a]*University of Washington, Seattle, USA*
[b]*European Center for Medium Range Weather Forecasts, Reading, UK*
[c]*University of Wisconsin, Madison, USA*

Abstract: The diurnal cycle of surface divergence over the oceans is examined using 4×daily data from the tandem SeaWinds satellite missions during April-September 2003. A statistically significant diurnal cycle of surface divergence is observed over a large fraction of the tropical and subtropical oceans. The highest amplitudes are found adjacent to tropical landmasses and decrease exponentially with distance away from the coast with a representative e-folding distance of approximately 200 km. In most of these near-coastal regions the surface divergence peaks at ∼15-20 hr local and there is evidence of offshore propagation of the signal. There are regions, however, where strong cycles persist for much greater distances offshore. Over the southeast Pacific Ocean, there is evidence of a diurnal subsidence wave that propagates for over 2000 km away from the South American coast at approximately 25 m s^{-1}. A cloud response to the subsidence wave moving westward from the Andes mountains is detected using passive microwave observations of liquid water path. Over the remote tropical Pacific, significant diurnal amplitude is found in and around regions of strong mean surface convergence with a phase suggesting a surface response to the early morning diurnal maximum in precipitation and propagation away from these sources consistent with gravity waves forced by deep tropospheric heating. ECMWF model simulations of 850 hPa subsidence show a diurnal cycle that is largely consistent with the SeaWinds divergence observations. Copyright © 2008 Royal Meteorological Society

KEY WORDS Surface divergence; diurnal; scatterometer; subsidence wave

Received 15 December 2007; Revised ; Accepted

1 Introduction

Large scale vertical motion in the lower atmosphere is associated with mean convergence/divergence of the surface winds. These convergence/divergence patterns can be detected over the oceans using satellite scatterometer data (Zheng et al., 1997) and yield a wide variety of information on vertical atmospheric motions occurring on a wide array of time and space scales. These can be useful both for the purposes of being able to better forecast weather systems (Atlas et al., 2001; Isaksen and Janssen, 2004) and for understanding dynamical processes occurring in the atmosphere (Chelton et al., 2004) and ocean (Kessler, 2002).

Single-satellite scatterometery provides some information on the diurnal cycle of ocean surface winds, but sampling is generally limited to twice daily at best. The SeaWinds tandem scatterometer missions (Lungu, 2002), however, allowed four-times daily sampling during a six month period (April-September 2003) with the same instrument design (SeaWinds) on two satellites (QuikSCAT at ∼06:00 and 18:00 hr local, and ADEOS-II at ∼10:30 and 22:30 hr local).

Scatterometer data have been used previously to study the diurnal cycle of surface winds using QuikSCAT alone (Gille et al., 2003) and using the tandem mission (Gille et al., 2005). These analyses revealed rich patterns of diurnal wind variability, including wind reversals in near-coastal regions that are clear signs of land/sea breeze circulations. The Gille et al. (2005) results also demonstrate a significant diurnal cycle of surface winds across most of the remote tropical Pacific and Atlantic Oceans. Using surface meteorological marine reports, Dai and Deser (1999) have suggested that the remote tropical ocean diurnal cycle is an equatorially-symmetric response to the diurnal cycle of tropical convection, but this conclusion is uncertain due to sampling noise.

In this paper we describe aspects of the diurnal cycle of surface divergence, rather than the wind components themselves, over the bulk of the global oceans using SeaWinds data complemented by vertical wind information from ECMWF analysis fields.

2 Methods

We use SeaWinds scatterometer wind measurements collected during April-September 2003. Input wind data are from the Jet Propulsion Laboratory Physical Oceanography Data Archive (PO-DAAC) and are gridded on a 0.25°×0.25° global grid. There is one grid for each of the ascending and descending passes from each of the QuikSCAT and ADEOS-II satellites. Data contaminated by rain are removed. These data are used to create, for each of the ascending and descending overpass grids for each satellite, mean wind maps at 0.25°×0.25° resolution for the six month period extending from 60°S to 60°N. Divergence fields are derived from these maps using centered differencing at the four overpass times.

*Correspondence to: Department of Atmospheric Sciences, Box 351640, University of Washington, Seattle, WA 98915, USA

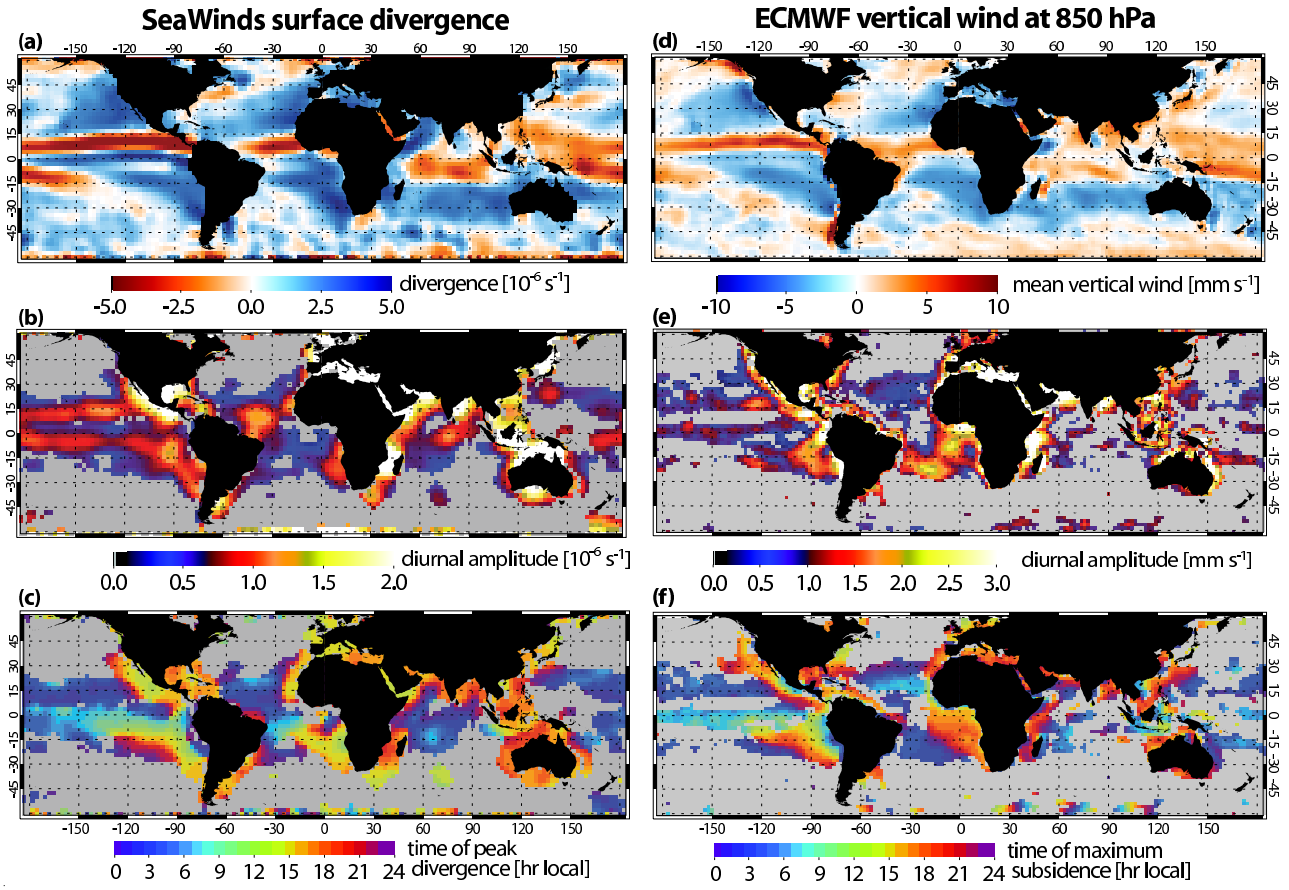

Figure 1: Mean, diurnal amplitude, and local time of maximum diurnal surface divergence for April-September 2003 from the tandem SeaWinds data (left panels). Mean, diurnal amplitude, and local time of maximum diurnal subsidence at 850 hPa from the ECMWF forecast data (right panels). Only regions for which the diurnal amplitude is statistically significantly different from zero at the 95% level are colored.

Next, to reduce noise we aggregate these data onto a $2.5°\times2.5°$ grid. The divergence diurnal cycle is analysed for each oceanic gridbox using a Fourier decomposition after first linearly interpolating the data temporally for the four mean overpass times (which vary with latitude) onto equally spaced local times (0, 6, 12, 18 hr). This decomposition yields the mean, amplitude and phase of the first diurnal harmonic. We do not use in this study the limited information about the semidiurnal cycle as it is poorly sampled with $4\times$ daily sampling, and therefore inconclusive.

A 10 day forecast using the 40km resolution European Center for Medium-Range Weather Forecasts (ECMWF) model was done for each of the six months (April-September 2003). Data was produces eight times per day (0, 3, 6, etc UTC) and then averaged in time and gridded using linear interpolation onto a $5°\times5°$ grid to deduce sampling noise. The key variable vertical velocity was specially diagnosed consistent with the semi-Lagranian advection to avoid the conversion of omega to vertical velocity, which is complicated by the semidiurnal tidal wave. Details are given in the Appendix. The model variable in this study is 850 hPa vertical wind field w_{850}, which is used to compare with the surface convergence data from SeaWinds which is itself regridded for the purpose onto a $5°\times5°$ grid. Quikscat surface winds are assimilated into the ECMWF variational analysis. Chelton and Freilich (2005) compared the ECMWF analyzed surface winds (with QuikScat) assimilation) to scatterometer and buoy data. They documented a 0.4 m s^{-1} wind speed low bias and rms model/QuikScat differences of 1.0-2.5 m s^{-1} with the lowest values in the trade wind regions such as those off the Chilean/Peruvian coast. This rms difference includes an estimated QuikScat random error of 0.75 m s^{-1} in the along-wind direction.

3 Results

3.1 Near global maps

Figure 1 shows maps of the mean surface divergence D_0, the diurnal amplitude, and the local time of maximum divergence from SeaWinds and the corresponding data for the 850 hPa subsidence rate from ECMWF. The mean divergence and subsidence fields clearly delineate the major features of the Boreal summer climatology including the extensive regions of divergence and corresponding subsidence over the eastern subtropical oceans, strongly convergent ITCZs in the eastern Pacific and Atlantic Oceans, the South Pacific Convergence Zone (SPCZ), and

DOI: 10.1002/qj

the broader regions of convergence and mean ascent in the tropical West Pacific and Indian Oceans. Regions of mean large scale midlatitude convergence are also evident, as are smaller scale convergence/divergence features especially in the Southern Ocean. These may be related to oceanic fronts and eddies that are quasi-stationary or move relatively slowly (Xie, 2004; Chelton et al., 2004; Small et al., 2008) compared with the six months of observations used here.

The diurnal amplitude (Fig. 1b) is largest close to coastlines, especially those in the tropics, exceeding 2×10^{-6} s^{-1} in many places, and comparable to the typical mean convergence rates. As with the mean fields, there is a good correspondence between strong divergence amplitude and strong 850 hPa subsidence amplitude in the ECMWF model, although there are some notable exceptions such as over the Atlantic Ocean. Especially over the region to the northeast of South America the regions of poor correspondence in the diurnal amplitude are also regions where the mean fields differ considerably.

The coastal diurnal cycle is far from uniform in amplitude. There are also extensive regions well away from coastlines with significant diurnal amplitude. For example, the region to the west of South America extending over 2000 km offshore has a large diurnal amplitude in both surface divergence and 850 hPa subsidence. In addition, significant amplitude exists in the narrow zones of strong convergence over the tropical Pacific, although this is more striking in the observations than in the EMCWF model fields. Few of the signals in midlatitudes are statistically significant in either the observations or the model. This does not necessarily preclude diurnal variability there, but reflects greater variability which reduces the signal to noise ratio. However, we note that the reduced Rossby radius in midlatitudes would also reduce the propagation distance for internal waves. A longer record than we currently have will be needed to determine if there are significant diurnal cycles in the midlatitudes.

Many of the broad features in Fig. 1b agree well with the analysis of ship and land station reports carried out by Dai and Deser (1999), but the amplitudes we observe are considerably greater by approximately a factor of two or so. The reason for this is unclear. Also, the improved sampling of the scatterometers compared with ships resolves some of the weaker but coherent features across the remote tropical Pacific and Southeast Pacific that are not clearly evident in the analysis of in-situ data.

In coastal regions the divergence and subsidence predominantly peaks in the afternoon and early evening (Fig. 1c,f), a pattern consistent with the land/sea breeze circulation (e.g. Rotunno, 1983) and supports the previous analysis from SeaWinds (Gille et al., 2005). We discuss this further in Section 3.3. In Section 3.4 we examine the interesting diurnal variability over the remote tropical Pacific.

An unexpected and interesting feature of Fig. 1(c,f) are the wave-like signals emanating from several stretches of the tropical coastlines that clearly propagate in time hundreds or even thousands of kilometers to the remote

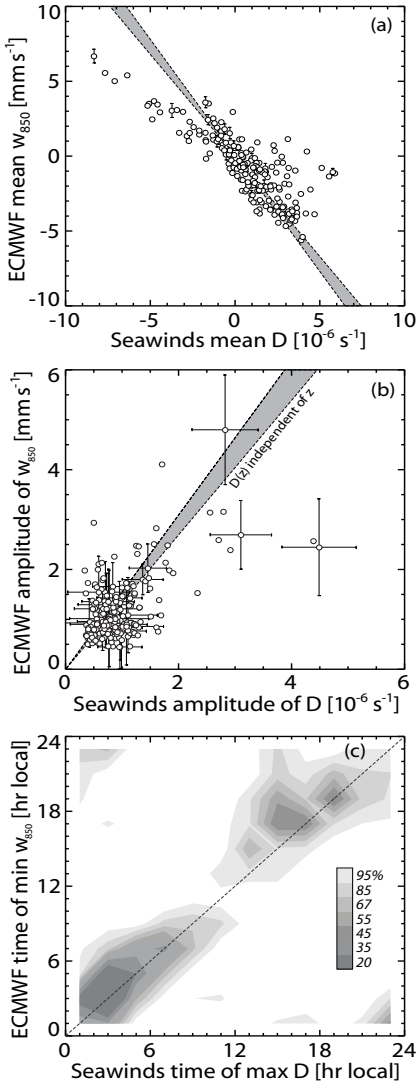

Figure 2: (a) Time-mean surface divergence D_0 from Seawinds against mean vertical wind at 850 hPa w_{850} from the ECMWF model. The data have been binned into $5^\circ\times5^\circ$ regions over the ocean (60°S-60°N) (b) As for (a) but a comparison of the amplitude of the diurnal cycle rather than the mean, and only those regions with an amplitude that is determined to be statistically distinguishable from zero at the 1-σ level are shown; The gray areas on (a) and (b) assume a constant divergence from the surface to 850 hPa, with the spread being that caused by variability in the height of the 850 hPa surface given seasonal and geographic variability in surface pressure and lower tropospheric temperature. Error bars represent sampling errors in the mean or the fitting error for diurnal amplitude, at the 1-σ level; (c) comparison of the phase of the diurnal cycle, i.e. a joint pdf of the Seawinds time of maximum D_0 and ECMWF time of minimum w_{850}, where the darkness of the grayscale indicates the density of points. The scale bar shows what fraction of the total joint pdf is contained in colors darker than the color indicated.

oceans. The most notable of these *subsidence waves* are seen over the Southeast Pacific and to the west of Mexico

DOI: 10.1002/qj

and Central America. We examine these waves in more detail in Section 3.5.

3.2 Divergence and vertical wind diurnal cycles

Figure 2 compares the time-mean, diurnal amplitude, and phase of the diurnal cycle of surface divergence (abscissae) with the respective time-mean, diurnal amplitude and phase of the 850 hPa vertical wind field (ordinates) from the ECMWF analyses. The mean fields are closely connected which is expected because the spatial variability of the time-mean surface divergence is a signature of the atmospheric general circulation which extends through the troposphere. Moreover the data are consistent with the idea that the mean divergence is roughly constant with height from the surface to 850 hPa in regions where the mean vertical velocity is relatively weak, and a divergence that decreases with height in regions of strong surface convergence (i.e. the ITCZ regions especially in the eastern Pacific and Atlantic, see Fig. 1). Assuming a quadratic vertical velocity profile one can infer the level $z_{\max}$ at which the vertical velocity must peak, i.e.

$$z_{\max} = \frac{1}{2}\frac{z_{850}}{(1-\frac{w_{850}}{D_0 z_{850}})} \qquad (1)$$

where z_{850} is the height of the 850 hPa level (approximately 1500 m). For strongly convergent regions (Fig. 2) $w_{850}/D_0 z_{850} \sim 0.5$ suggesting that $z_{\max}$∼1500 m. Interestingly, this is close to the height of maximum vertical velocity for strongly convergent regions of the eastern Pacific found in Back and Bretherton (2006).

While the diurnal amplitudes are significantly correlated (r=0.60, Figure 2b), sampling noise is substantially greater than for the mean state. However, a comparison of the phase of the diurnal cycle (Figure 2c) reveals that the diurnal cycle of w_{850} and that of surface divergence are in phase suggesting that the diurnal signals in the scatterometer data are consistent with a mode of diurnal variability extending above the boundary layer. Indeed, the phases of w_{850} and D_0 remain in good agreement at 700 hPa but the agreement is much poorer at 500 hPa (not shown) suggesting that the processes responsible for the diurnal cycle in surface divergence are generally confined to the lowest half of the troposphere.

3.3 Near-coastal diurnal cycle

Figure 3 demonstrates that equatorward of 30° N and S the regions where the diurnal amplitude in D_0 is strongest are most frequently found to be within 4-5° of the coast, and that in these regions D_0 most typically peaks during the late afternoon. This is consistent with the expected pattern for a sea-breeze circulation, and is behavior consistent with Gille et al. (2005). The strength of the surface sea-breeze response decreases approximately exponentially with distance away from the coast with an e-folding distance of approximately 200 km. This is consistent with the linear theory of the sea breeze as elucidated by Rotunno (1983), where for latitudes equatorward of 30° the horizontal influence of the sea breeze circulation extends to a distance $L = NH(\omega^2 - f^2)^{-1/2}$, where N is the Brunt-Vaisala frequency, H is the depth of the heating, ω is the diurnal frequency, and f is the Coriolis parameter. For a 1 km deep heating typical of the sea-breeze circulations around relatively flat coastlines the value of L increases from about 150 km at the Equator to about 300 km at 20°N and S. These values are consistent with the 200 km e-folding distance for the amplitude of the near-coastal observations in Figure 3b, but breakdown of the observations by latitude did not reveal any significant latitudinal variations from 30°S to 30°N. It is unclear why this is.

Another interesting feature of the near-coastal diurnal cycle is that there is considerable geographical variability in the amplitude, with the strongest cycles being found in regions where the coastline is relatively convex on length-scales of up to a few times the e-folding distance (Fig. 1b,e). For example, while regions such as the Gulf of Mexico, the Arabian Gulf, between Madagascar and mainland Africa have very strong amplitudes, other regions such as the much of the eastern coast of South America, far eastern and western coasts of Australia, and South Africa, with more concave coastlines, do not exhibit such strong diurnal variability. The constructive interference of multiple land-sea breezes is hypothesized to be responsible for such behavior.

Other near-coastal regions in the tropics show remarkably weak diurnal variability in surface divergence. The Brazilian coastline and the Gulf of Guinea are two such areas (Fig. 1b). It is curious that in both of these regions ECMWF shows significant diurnal amplitude in the vertical wind, inconsistent with the generally tight relationship between the diurnal cycle of surface divergence and wind discussed in Section 2.2. In both these regions, the prevailing flow is predominantly onshore during April to September, which observations suggest can impact the propagation speed and spatial structure of the sea-breeze circulation (Atkins and Wakimoto, 1997). A more detailed analysis of the impact of prevailing flow is beyond the scope of this study.

3.4 Tropical remote ocean

Figure 4 shows that over the remote tropical oceans, where the influence of land is minimal, regions with mean surface convergence tend to exhibit a strikingly different diurnal cycle from divergent regions. In most convergent regions D_0 tends to peak between 2 and 6 am local time. In divergent regions the time of peak divergence tends to be more evenly distributed throughout the day. Having said this, it may be notable that there is still a preference for D_0 to peak during the later night and early morning hours in divergent regions, and at a delayed hour compared with convergent regions.

The data in Figure 1(c) are consistent with an analysis of surface divergence from Tropical Pacific surface wind measurements within 8° of the equator (Deser and Smith, 1998). Both show surface divergence peaking at approximately 08 local time. Our results indicate that this reflects

DOI: 10.1002/qj

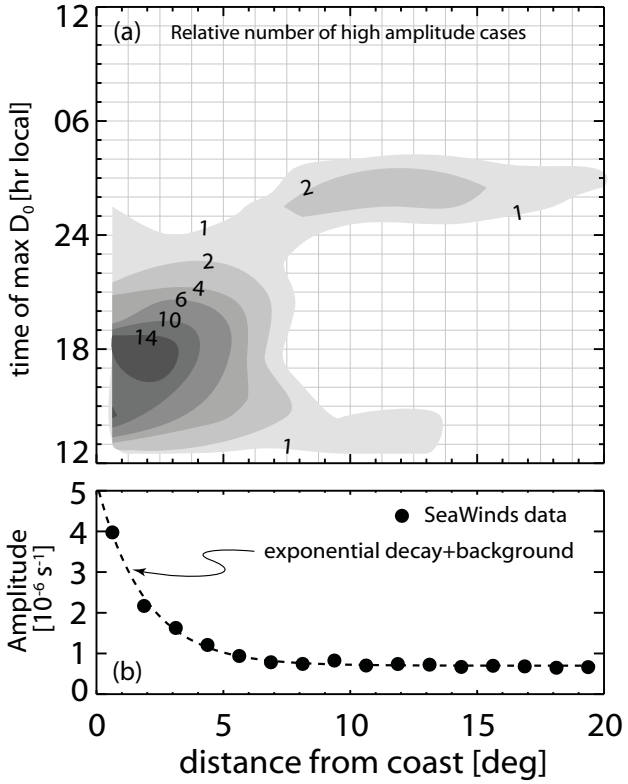

Figure 3: (a) The number of 2.5°×2.5° regions, in the tropics (30°S-30°N), that have a statistically significant and strong (amplitude greater than 10^{-6} s^{-1}) diurnal cycle of D_0 with a given phase (1 hour intervals) as a function of the distance from the nearest coastline; (b) the mean amplitude of the diurnal cycle for all locations with a statistically significant diurnal cycle in D_0 as a function of distance from the coast. The dashed line shows an exponential decay with an e-folding distance of 1.9°, and a far-field amplitude of 0.7×10^{-6} s^{-1}.

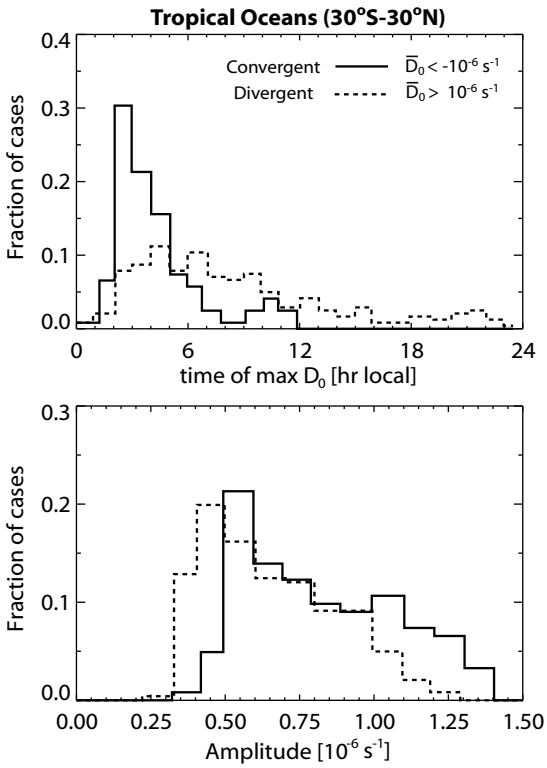

Figure 4: (a) Histograms of the time of maximum D_0 and (b) the diurnal D_0 amplitude for 2.5°×2.5° regions with statistically significant diurnal cycles over the remote (>20° from the nearest coast) tropical (30°S-30°N) oceans. Different histograms are shown for regions where the mean $D_0>10^{-6}$ s^{-1} (divergent regions, dashed lines) and where $D_0<$-10^{-6} s^{-1} (convergent regions, solid lines).

the time taken for the diurnal wave to propagate from its source (the ITCZ).

Whether this behavior is consistent with the idea of diurnal strengthening and weakening of the Hadley cells, as suggested by the analysis of ship surface wind reports in Dai and Deser (1999), is not clear. Insofar as the diurnal cycle of surface divergence can be interpreted in this way, a comparison of the diurnal amplitude with the mean convergence indicates that the oceanic Hadley cell may undergo a diurnal cycle with an amplitude of some 10-20% of the mean. From the scatterometer data (Fig. 4) it is inferred that the Hadley cell would be weakest during the early morning hours, which contrasts with the late evening weakening suggested by the analysis of Dai and Deser (1999). However, the spatial smoothing used in Dai and Deser (1999) to reduce noise may have resulted in a loss of the intricate spatial variability that is revealed by the scatterometer data.

Precipitation, and therefore convective heating from oceanic tropical deep convection peaks during the late evening and early morning hours (e.g. Nesbitt and Zipser, 2003; Yang and Smith, 2006). The behavior in Fig. 4 appears consistent with the generation of diurnal gravity waves by deep convective heating which then propagate away from the heat sources to adjacent regions of mean subsidence.

A striking example of propagating waves from deep convection can be seen by examination of the region to the south of the East Pacific ITCZ (110-130°W) in Fig. 1. In the ITCZ region itself (7-16°N) the peak D_0 occurs during the early morning hours. The peak D_0 becomes progressively later as one moves south over the divergent regions, finally peaking during the late evening at 20°S, 110-120°W where on its eastern edge it merges with the southeast Pacific wave (see Section 3.5.2 below). This propagation speed is ∼50 m s^{-1} consistent with an internal wave (see section 3.3) caused by heating extending up to approximately 13 km. This is in excellent agreement with the depth of convective latent heating for tropical deep convection which peaks at about 7-8 km and extends to 12-14 km (Shige et al., 2007).

3.5 Diurnal subsidence waves

The previous two subsections have explored the diurnal subsidence and vertical wind variability found in many the

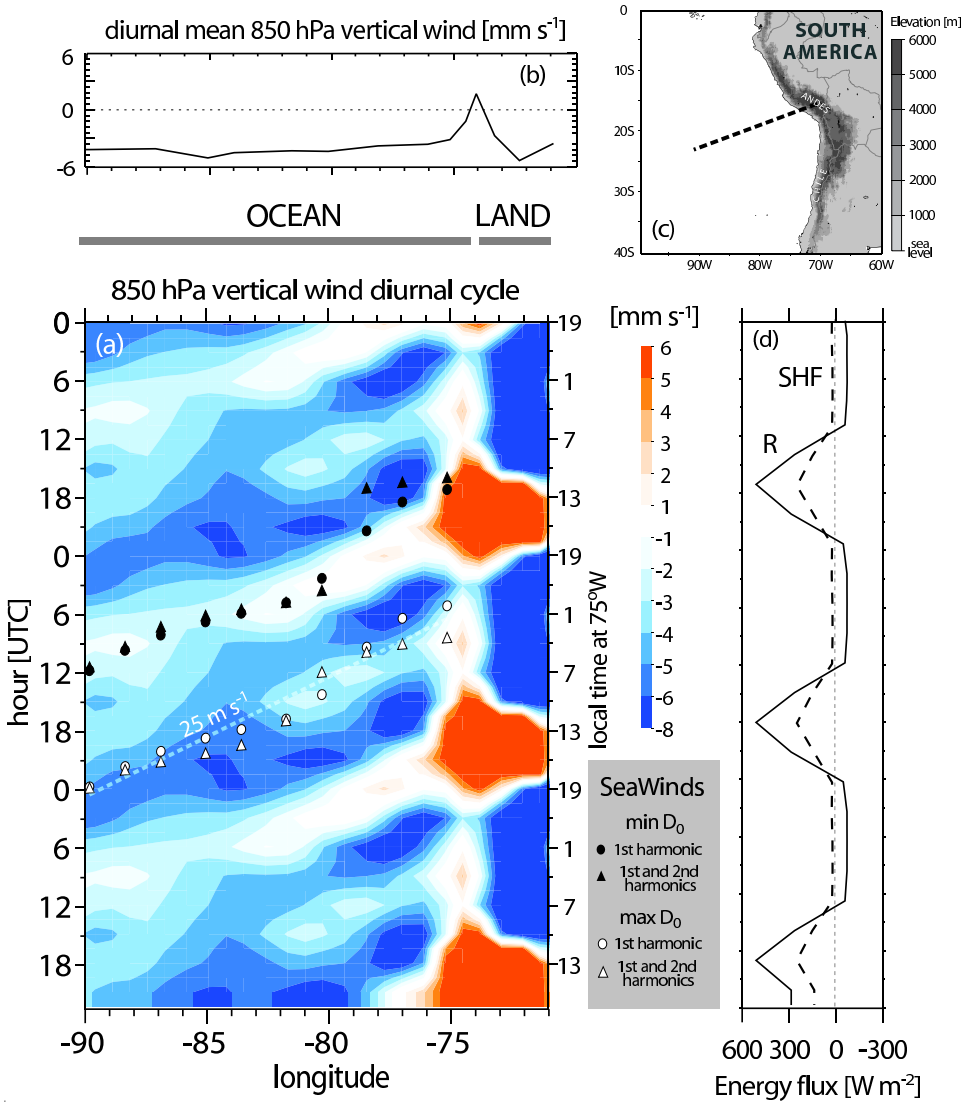

Figure 5: (a) Diurnal Hovmöller plot of w_{850} (colors) from ECMWF analyses along the line joining 23°S, 90°W and 15°S, 72°W; also shown are the times at which the scatterometer data indicates minimum (black) and maximum (white) surface divergence based on either 1st harmonic alone (circles) or on the 1st and 2nd harmonics (triangles); the diurnal cycle is repeated three times for clarity; (b) Diurnal mean vertical wind at 850 hPa from ECWMF; (c) geographic location with orography shown; (d) Mean sensible heat flux (SHF) and net radiative flux from the ECMWF analyses at a location (15°S, 72°W) on the western Andean slopes as a function of time. Local time at 75°W is UTC time minus 5 hrs.

near-coastal and remote tropical oceanic regions. However, examination of Fig. 1 reveals several regions for which it is difficult to explain the diurnal variability with either classical land-sea breeze dynamics or with gravity wave production from tropical oceanic deep convection. Two such regions are to the south and west of the Central American coast, and the southeast Pacific west of Chile and Peru.

3.5.1 *Central American coast*

Stretching from the Pacific waters adjacent to the Baja Penninsula, to Nicaragua, is a region with a particularly strong diurnal cycle (Fig. 1(b,e)), which extends at least 10°from the coast. Close to the coast peak divergence is found in the early afternoon, consistent with the seabreeze circulation, if a little earlier than many other near-coastal regions (Fig. 3). The coastline here is not concave, and there is strong mean convergence and upward vertical velocity as it is a region of strong deep convection during the summer months (Fig. 1(a,d)). It is possible that in this region the deep convection helps to amplify the effect of the seabreeze with a gravity wave mechanism of Mapes et al. (2003).

3.5.2 *Southeast Pacific*

The southeast Pacific diurnal subsidence wave seen in Fig. 1 is associated with the diurnal heating of the western slopes of the Andes Cordillera, which rise to a mean

DOI: 10.1002/qj

height of more than four kilometers over a distance of several thousand kilometers. The wave has been the focus of a numerical model study (Garreaud and Muñoz, 2004) which suggested that the wave is a propagating gravity wave extending up to approximately 5-6 km above the surface, and propagating well over 1000 km from the coast. Our observations confirm that the wave structure is coherent even at 90°W, approximately 2000 km from the South American coast.

Figure 5 shows a Hovmöller plot along a line approximately perpendicular to the phase lines, i.e. along the direction of propagation of the subsidence wave. The time of maximum D_0 from the scatterometer coincides fairly well with the maximum downward vertical motion (strongest subsidence) demonstrating that the ECMWF model appears to capture the essence of the subsidence wave. The estimated wave propagation speed is approximately 25 m s^{-1} and is consistent with the model-derived value of $\sim$30 m s^{-1} reported in Garreaud and Muñoz (2004). The propagation speed c is related to the depth of the heating H, and the mean buoyancy frequency at levels below the heating N, via $c = NH/\pi$ (Holton, 1992; Nicholls et al., 1991). A reasonable depth for the convective dry heating on the Western Andean slopes is $H =$ 6 km (the Andes range in the region of interest itself rises to 4-5 km), and with $N \approx 0.012$ s^{-1} throughout most of the tropical and subtropical low to mid troposphere, this leads to gravity wave propagation speeds of $\sim$23 m s^{-1} consistent with the observations.

The observed wave phase is also in excellent agreement with that simulated by Garreaud and Muñoz (2004) and from the idealized simulations of Nicholls et al. (1991), with the time of maximum subsidence and surface divergence at any given distance from the coast connected to the time of maximum heating by the wave propagation speed. Thus, the maximum divergence at 75°W occurs about 3-4 hours or so after the time of maximum heating on the Andes (the crest of which is located at 72°W along the cross section line used to construct the Hovmöller plot) consistent with a propagation speed of $\sim$25 m s^{-1} ($\sim$1° hr^{-1}). The scatterometer data and ECMWF data therefore provide support for a regionally extensive diurnal subsidence wave extending over a broad region of the Southeast Pacific ocean.

The model simulations of Garreaud and Muñoz (2004) also suggest that the wave strengthens the diurnal cycle of cloudiness over the stratocumulus-capped marine boundary layer (MBL) to the west of South America. This may help to explain why the diurnal cycle of cloud liquid water path in this region is the strongest of any of the regions of persistent subtropical low cloud (Wood et al., 2002). The simulations also demonstrate that the wave amplitude is greatest during the Austral summer, and so the scatterometer data used here (April-September 2003) is providing observations of the wave during its weakest season.

In remote subtropical oceanic regions dominated by low clouds the peak cloud liquid water path (LWP) is observed to occur at 3-5 am local time (see e.g. Table 1 in Wood et al., 2002) consistent with daytime stabilization of the MBL by solar absorption in the cloud layer. This causes the MBL to decouple thereby reducing the moisture supply to the cloud (Turton and Nicholls, 1987). To examine the diurnal cycle of LWP, we use data taken from a University of Wisconsin passive microwave climatology of cloud LWP O'Dell et al. (2008) which uses a robust methodology to seamlessly combine LWP data from all available microwave imagers from 1988 to the present, starting from the retrieved LWP values from individual satellites using the retrieval algorithm of Hilburn and Wentz (2008). The climatology contains monthly mean values and corresponding diurnal cycles of LWP over the global oceans, as well as error estimates on all derived quantities based on the known statistical and systematic error sources.

To elucidate the propagating features in the LWP, we remove from the diurnal cycle of LWP (Apr-Sep) at each longitude the diurnal cycle of LWP at 20°S, 90°W. This location is sufficiently far from the shore that the diurnal cycle here represents primarily the effect of the solar absorption during the daytime. The amplitude (half of the maximum minus the minimum) of the diurnal cycle at 20°S, 90°Wis close to 25 g m^{-2}, peaking at approximately 3 am local time. Figure 6 shows diurnal Hovmöller plots (time of day vs longitude) of these diurnal LWP anomalies, along the line shown in Fig. 5. Clearly propagating features are apparent in the anomalies, with speeds roughly consistent with the speed of the diurnal subsidence waves observed in Seawinds data and the ECMWF data, suggesting a link between the propagating waves and the cloud LWP. The amplitude of the propagating component of the diurnal LWP cycle is comparable to that of the remote ocean diurnal cycle at 20°S, 90°W. At 75-80°W the anomalous LWP peaks during the late afternoon/early evening and thus results in a partial cancellation of the diurnal cycle due to solar absorption.

These results are consistent, at least qualitatively, with the interference of the diurnal subsidence with the diurnally-modulated solar absorption. Enhanced subsidence impacts the cloud by lowering the cloud top height thus thinning the cloud. Conversely a minimum in subsidence (which at certain times of the day even becomes net ascending motion in this region) results in a deepening of the boundary layer and a tendency towards thicker clouds. Landward of 80°W, upward motion during the afternoon appears to be sufficient to significantly deepen the boundary layer. The *rate of deepening* is maximal when the subsidence is minimal, and so the deepest boundary layer would occur some time after this (6 hours for a truly sinusoidal diurnal wave). So, by late afternoon this results in the enhanced diurnal anomaly in LWP seen in Fig. 6. This LWP anomaly occurs at later times further from the land consistent with the propagation of the diurnal subsidence wave. In addition, near the coast the enhanced subsidence during the early morning suppresses the early morning LWP peak.

By the time the wave is further from shore, its effect is to enhance the diurnal cycle caused by solar absorption

DOI: 10.1002/qj

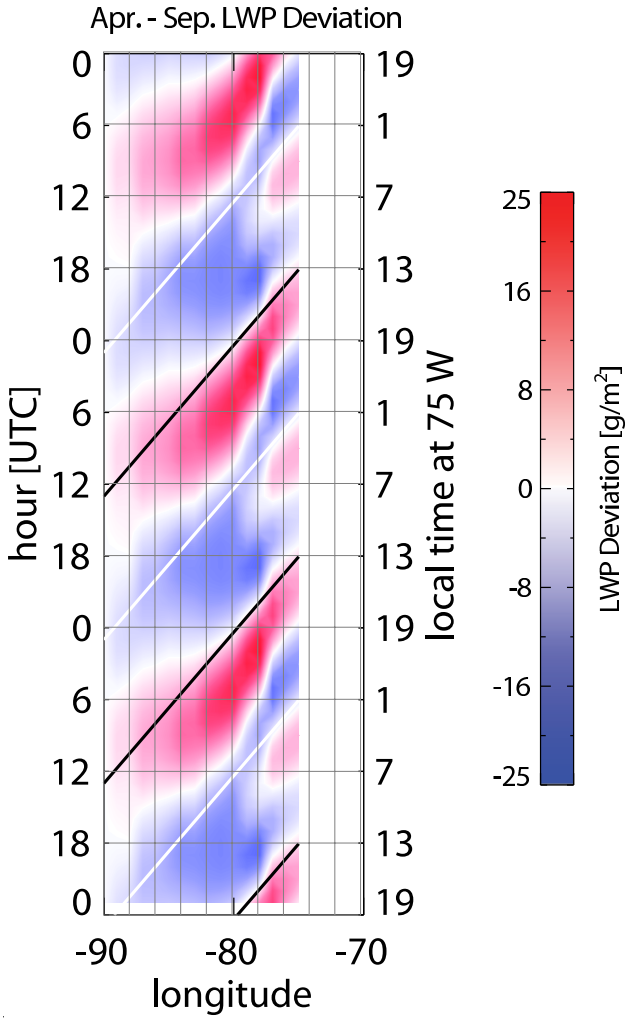

Figure 6: Hovmöller of LWP diurnal anomalies for April-July along the same line as in Fig. 5 from the passive microwave climatology of O'Dell et al. (2008). To calculate the anomalies, the mean diurnal cycle at 20°S, 90°W(the far-field diurnal cycle) was removed from the diurnal cycle at each longitude. The white line reproduces the line of maximum subsidence shown in Fig. 5 and the black line is the approximate time of the minimum subsidence.

alone because the minimum subsidence rate occurs around midnight (e.g. at 85°W) where it would help deepen the MBL during the night and enhance the existing modulation of MBL depth and cloud. This is clearly seen in the positive LWP anomalies during the early morning hours at 85°W in Fig. 6. This is also supported by surface remote sensing observations at 20°S, 85°W taken during the EPIC field program (Bretherton et al., 2004; Caldwell et al., 2005) which show a very strong diurnal cycle of MBL depth in this region that is enhanced by constructive interference of the solar absorption and the diurnal subsidence.

What does seem clear is that the diurnal subsidence wave has the ability to affect the diurnal cycle of cloud properties at large distances from the South American coast. More work will be required to examine its impact upon the diurnally averaged solar insolation at the ocean surface and therefore the climate of the region.

4 Discussion and Conclusions

The 4×daily scatterometer data examined here reveal a rich pattern of diurnal variability extending over a large fraction of the world's oceans. It is natural to expect that the Coriolis force would limit the horizontal distance over which internal waves can propagate, which helps to explain why the remote oceanic diurnal features are largely confined to the region within 20-30° of the Equator (Fig. 1). However, the six month limits of the data record effectively rule out the detection of diurnal signals in regions of strong synoptic variability. Analyses of longer records (e.g. Dai and Deser, 1999) may be useful but lack the coverage that the scatterometer data can give.

The diurnally-varying surface convergence is the signature of a diurnal cycle of vertical motion extending through a significant part of the lower troposphere. Subsidence in the lower troposphere relates to surface divergence by continuity. The significant agreement of the mean value and phase between ECMWF subsidence at 850 hPa and SeaWinds surface divergence (Fig. 2) adds confidence in the accuracy of the mean and diurnal cycle of each of the two datasets. In some regions these motions appear to be sufficiently strong to significantly alter the diurnal cycle of cloud liquid water content. Even if the mean LWP is unchanged by this diurnal dynamic variability there may be rectification of the solar cycle with impacts on the upper ocean heat budget in coastal regions. For example, over the SE Pacific, where the strong diurnal subsidence wave is observed, in the region out to 500-700 km from the coast, our results imply that the clouds may be more reflective during the daytime hours when the solar radiation is strongest than they would otherwise have been without the subsidence wave. This would result in a reduced solar flux at the surface which would cool the surface waters thus enhancing the cooling due to oceanic upwelling. Observations of the diurnal cycle of cloud cover (rather than LWP) would be required to quantify this contribution of the Andes to upper ocean cooling, but it is likely to be a significant effect which would additionally help to explain the extensive region of cold sea surface temperature to the west of South America (Takahashi and Battisti, 2007).

In addition to the potential effects of the subsidence wave on the climatology of the SE Pacific, we hypothesize that there may also be a connection between the waves and the transition from closed to open cellular convection, which occurs mainly at night (Wood et al., 2008). By enhancing the LWP, the enhanced thickening of the MBL caused by the subsidence wave during the late evening and early morning observed westward of 79°W would also add additional fuel to nocturnal precipitation formation which is understood to be intimately connected with the formation of open cells (Stevens et al., 2005).

Finally, we have demonstrated that the diurnal cycle of surface convergence is a useful test for the ability of

DOI: 10.1002/qj

global models to accurately represent physical processes throughout the tropics. It would be a fruitful endeavor to combine the various extensive scatterometer datasets over the previous two decades to generate a dataset focused upon diurnal variability.

Acknowledgements

We thank Rene Garreaud for valuable discussions on the nature of the diurnal cycle over the southeast Pacific Ocean. Nils Wedi at ECMWF developed the novel vertical velocity diagnostic analysis used in this work. This work was supported in part by NSF Grant 0433712. AMSR-E data are produced by Remote Sensing Systems and sponsored by the NASA Earth Science REASoN DISCOVER Project and the AMSR-E Science Team. Data are available at http:// www.remss.com. QuikScat data are produced by Remote Sensing Systems and sponsored by the NASA Ocean Vector Winds Science Team.

5 Appendix: Calculation of vertical velocity from ECMWF forecast fields

Calculation of vertical velocity w from the default model output of omega ($\omega = \frac{dp}{dt}$) is complicated by the presence of pressure waves such as the semi-diurnal tidal wave prevalent in the tropics (Andrews et al., 1987; Janssen, 1999). This complication can be demonstrated by writing w in the pressure coordinate system

$$w = \frac{dz}{dp} \tag{2}$$

$$= \frac{\partial z}{\partial t}\Big|_p + v_p \cdot \nabla_p z + \omega \frac{\partial z}{\partial p} \approx \frac{\partial z}{\partial t}\Big|_p \tag{3}$$

$$+ v_p \cdot \nabla_p z - \frac{\omega}{\rho g} \tag{4}$$

The last equation uses the hydrostatic equation. The second term is negligible for tidal waves because of their horizontal length scales of ~ 20000km. The difficulty of ω to w conversion then lies in the determination of the pressure surface variations, i.e. the first term, such as tidal waves.

Therefore, the vertical velocity was specially diagnosed consistent with the semi-Lagrangian advection scheme used in the ECMWF model (see Temperton and Staniforth (1987) for a description of the numerical formulation). The vertical velocity at the trajectory mid-point $w^{1/2}$ between arrival and departure points z^+ and z^0 in this framework is written as

$$w^{1/2} = \frac{1}{2}(w^+ + w^0) = \frac{z^+ - z^0}{\Delta t}. \tag{5}$$

where z^+ is at a grid point and z^0 is found by interpolation of the geopotential to the departure point of the semi-Lagrangian trajectory. Equation (5) is solved for the vertical velocity and the arrival point w^+.

References

Andrews, D. G., J. R. Holton, and C. B. Leovy, 1987: *Middle atmosphere dynamics*. Academic Press.

Atkins, N. T. and R. M. Wakimoto, 1997: Influence of the synoptic-scale flow on sea breezes observed during CaPE. *mwr*, **125**, 2112–2130.

Atlas, R., et al., 2001: The effects of marine winds from scatterometer data on weather analysis and forecasting. *Bull. Am. Meteor. Soc.*, **82**, 1965–1990.

Back, L. E. and C. S. Bretherton, 2006: Geographic variability in the expore of moist static energy and vertical motion profiles in the tropical Pacific. *Geophys. Res. Lett.*, **33**, L17 810, doi:10.1029/2006GL026 672.

Bretherton, C. S., T. Uttal, C. W. Fairall, S. E. Yuter, R. A. Weller, D. Baumgardner, K. Comstock, and R. Wood, 2004: The EPIC 2001 stratocumulus study. *Bull. Am. Meteor. Soc.*, **85**, 967–977.

Caldwell, P., R. Wood, and C. S. Bretherton, 2005: Mixed-layer budget analysis of the diurnal cycle of entrainment in SE Pacific stratocumulus. *J. Atmos. Sci.*, **62**, 3775–3791.

Chelton, D. B. and M. H. Freilich, 2005: Scatterometer-based assessment of 10m wind analyses from the operational ECMWF and NCEP numerical weather prediction models. *Mon. Wea. Rev.*, **133**, 409–429.

Chelton, D. B., M. G. Schlax, M. H. Freilich, and R. F. Milliff, 2004: Satellite measurements reveal persistent small-scale features in ocean winds. *Science*, **303**, 978–983.

Dai, A. and C. Deser, 1999: Diurnal and semidiurnal variations in global surface wind and divergence fields. *J. Geophys. Res.*, **104**, 31 109–31 125.

Deser, C. and C. A. Smith, 1998: Diurnal and semidiurnal variations of the surface wind field over the tropical pacific ocean. *J. Climate*, **11**, 1730–1748.

Garreaud, R. D. and R. Muñoz, 2004: The diurnal cycle in circulation and cloudiness over the subtropical southeast Pacific: A modeling study. *J. Climate*, **17**, 1699–1710.

Gille, S. T., S. G. L. Smith, and S. M. Lee, 2003: Measuring the sea breeze from quikscat scatterometry. *Geophys. Res. Lett.*, **30 (3)**, Art No. 1114.

Gille, S. T., S. G. L. Smith, and N. M. Statom, 2005: Global observations of the land breeze. *Geophys. Res. Lett.*, **32**, L05 605, doi:10.1029/2004GL022 139.

Holton, J. R., 1992: *An introduction to dynamic meteorology*.

Isaksen, L. and P. A. E. M. Janssen, 2004: The benefit of ERS scatterometer winds in ECMWF's variational assimilation system. *Q. J. R. Meteorol. Soc.*, **130**, 1793–1814.

Janssen, P. A. E. M., 1999: On tides in the ecmwf model. ECMWF Technical Memorandum 284, European Centre for Medium-Range Weather Forecasts.

Kessler, W. S., 2002: Mean three-dimensional circulation in the northeast tropical Pacific. *J. Phys. Oceanogr.*, **32**, 2457–2471.

Lungu, T., 2002: Seawinds science data product user's manual, version 1.0. Tech. Rep. JPL Doc D-21551, 128 pp, NASA Jet Propulsion Laboratory, Pasadena, Calif.

Mapes, B. E., T. T. Warner, and M. Xu, 2003: Diurnal patterns of rainfall in northwestern south america. part iii: Diurnal gravity waves and nocturnal convection offshore. *Monthly Weather Review*, **131 (5)**, 830–844.

Nesbitt, S. W. and E. J. Zipser, 2003: The diurnal cycle of rainfall and convective intensity according to three years of trmm measurements. *J. Climate*, **16**, 1456–1475.

Nicholls, M. E., R. A. Pielke, and W. R. Cotton, 1991: Thermally forced gravity waves in an atmosphere at rest. *J. Atmos. Sci.*, **48**, 1869–1884.

O'Dell, C. W., F. J. Wentz, and R. Bennartz, 2008: Cloud liquid water path from satellite-based passive microwave observations: a new climatology over the global oceans. *J. Climate*, submitted.

Rotunno, R., 1983: On the linear theory of the land and sea breeze. *J. Atmos. Sci.*, **40**, 1999–2009.

Shige, S., W. K. Takayabu, W. K. Tao, and C. L. Shie, 2007: Spectral retrieval of latent heating profiles from TRMM PR data. Part II: Algorithm improvement and heating estimates over tropical ocean regions. *J. App. Met. Climatol.*, **46**, 1098–1124.

Small, R. J., et al., 2008: Air-sea interaction over ocean fronts and eddies. *Dyn. Atmos. Oceans*, 274–319, small, R. J. deSzoeke, S. P. Xie, S. P. O'Neill, L. Seo, H. Song, Q. Cornillon, P. Spall, M. Minobe, S. 189 356QS.

Stevens, B., G. Vali, K. Comstock, R. Wood, M. VanZanten, P. H. Austin, C. S. Bretherton, and D. H. Lenschow, 2005: Pockets of open cells (POCs) and drizzle in marine stratocumulus. *Bull. Am. Meteor. Soc.*, **86**, 51–57.

Takahashi, K. and D. S. Battisti, 2007: Processes controlling the mean tropical pacific precipitation pattern. Part I: The Andes and the eastern Pacific ITCZ. *J. Climate*, **14**, 3434–3451.

Temperton, C. and A. Staniforth, 1987: An efficient two-time-level semi-Lagrangian semi-implicit integration scheme. *Q. J. R. Meteorol. Soc.*, **57**, 2656–2670.

Turton, J. D. and S. Nicholls, 1987: A study of the diurnal variation of stratocumulus using a multiple mixed layer model. *Q. J. R. Meteorol. Soc.*, **113**, 969–1009.

Wood, R., C. S. Bretherton, and D. L. Hartmann, 2002: Diurnal cycle of liquid water path over the subtropical and tropical oceans. *Geophys. Res. Lett.*, **10**, 1029/2002GL015 371.

Wood, R., K. K. Comstock, C. S. Bretherton, C. Cornish, J. Tomlinson, D. R. Collins, and C. Fairall, 2008: Open cellular structure in marine stratocumulus sheets. *J. Geophys. Res.*, **17**, in press.

Xie, S. P., 2004: Satellite observations of cool ocean-atmosphere interaction. *Bulletin of the American Meteorological Society*, **85 (2)**, 195–+.

Yang, S. and E. A. Smith, 2006: Mechanisms for diurnal variability of global tropical rainfall observed from TRMM. *J. Climate*, **19**, 5190–5226.

Zheng, Q. A., X. H. Yan, W. T. Liu, W. Q. Tang, and D. Kurz, 1997: Seasonal and interannual variability of atmospheric convergence zones in the tropical Pacific observed with ERS-1 scatterometer. *Geophys. Res. Lett.*, **24 (3)**, 261–263.